Modal modification of structural damping applied to increase the stability and convergence of numerical integration

Krzysztof Lipiński

Gdańsk University of Technology, Faculty of Mechanical Engineering and Ship Technology, Institute of Mechanics and Machine Design
ul. Narutowicza 11/12, Gdańsk, 80-233, Poland
klipinsk@pg.edu.pl

Keywords: structural damping, modal adjustment, multibody and finite elements, stability of numerical integration

1 Introduction

This text refers to numerical analyses completed on systems fused of multibody and finite-element parts. The presence of its multibody part leads to nonlinear formulae, i.e., nonlinear formulae express the second-order differential equations of their dynamics. Standardly, to solve such equations, one shall use one of the standard "step-by-step" integration algorithms, and when one is using these algorithms, the one approximates the initial nonlinear systems of differential equations by their associated sets of finite difference equations. According to these approximations, the obtained answers does not fully correspond to the real time evolutions of the original system. They contain both, an outline of the real evolution, and redundant/superfluous solutions, unrelated to the true one. These last ones shall be considered as the approximation errors. Designers of algorithms try to find robust processes that does not magnify these errors. Such algorithms are called numerically stable, and they do not produce extraordinarily different results for tiny changes in the initial data. We should underline that this instability is a phenomenon resulting of the employed algorithm, but not due to the problem itself.

In the examined tests, the investigated simultaneous presence of the inertial and elastic components leads to the creation of a vibrating system. We assumed, that the damping only results from a structural damping set in finite-element part. In this tests we try to check, if the increase in damping can't cause problems with the stability of numerical integration

If we focus on problems associated with the finite-elements models, the accurate modelling of the damping matrix, C_c, is an intricate problem, mainly due to the complexity of the physical phenomena and due to limitations in identifications of the related parameters. As a result, only the general properties are known or detectable. According to the acceptance of the necessity of simplifications, basic models are dominant, and one can classify the uniform Rayleigh model and modal damping as the most popular simplified models. The Rayleigh damping matrix [1, 2, 3, 4, 5, 6-8] (also called proportional or classical damping matrix) is a linear combination of the stiffness and mass matrices,

$$C^c = \alpha \cdot M^c + \beta \cdot K^c \ . \tag{1}$$

where: $M^c = const - n_c \times n_c$ mass matrix of the finite-element part; $C^c = const - n_c \times n_c$ damping matrix of the finite-element part; $K^c = const - n_c \times n_c$ elasticity matrix of the finite-element part;

In general, Rayleigh's parameters, α and β, are small numbers ($\alpha=3.98 \times 10^{-4}$ and $\beta=0.94$, or $\alpha=0$ and $\beta=3.23 \times 10^{-3}$ [8]). Of course, we shall treat eq. (1) as the canonical version of the formula (e.g., Hall [9] suggested excluding the mass-proportional part of the formula and binding the stiffness-proportional part of the Rayleigh formula). Moreover, let us underline that, when transferring the dynamics from the nodal coordinates to the modal ones, the Rayleigh model leads us to diagonal modal damping matrices, i.e., the resulting equations in modal coordinates are independent of each other, and a single factor expresses damping in each of these modes. Unfortunately, even if one uses small Rayleigh parameters, the resulting number of the decaying oscillations is low. The dominant ones are the purely decaying modes expressed by high-moduli real-number eigenvalues. Mathematical analyses confirm that they reduce rapidly and stabilize at their zero values. We can observe similar effects in the outcomes of material experiments and in results of numerical calculations.

Following the literature, we can find several algorithms that try to omit the problem, e.g., the troublesome modes are detected and eliminated from the model. Such algorithms are named *modal coordinate reduction algorithms* [5, 10, 11]. They constitute one of the most extensively used techniques of reduction, applicable for linear and weakly non-linear systems. The number of related publications is high. The works cited above are exemplary. Focusing on its canonical version, it combines two steps: the mode superposition and the modal truncation [5]. The second step removes all those modes that have an insignificant contribution to the potential responses of the system. Accordingly, a small part of the primary (dominant/master) modes, while the others (slave modes) are truncated [11]. Selection of the truncated modes is not a straightforward problem. Except for the modal reduction, it also looks attractive to adjust Rayleigh parameters individually to each of the modes. It is the second of the most-popular attempts. In this attempt, the resulting matrix of the modal damping is a user-selected diagonal matrix with individually fitted ratios. These ratios can be got experimentally or assumed. Uniform modal damping is the best-known theoretical option. If focusing on the paper-investigated system, the implemented Rayleigh model results in only 12 vibrational/oscillatory modes of the beam dynamics. The others (about 90 modes) refer to purely decaying motions resulting from real eigenvalues. Its highest eigenvalue is higher than 10^8. Such processes, if excited, are problematic for material observation and for numerical integration. They require extremely short time steps.

We divided this paper into eight sections. The one that directly follows the introduction presents the fundamentals of the used multibody formalisms. Section three presents a brief background of the finite-element method. The fourth section

presents the paper proposed constraint equations. It also focuses on the paper-proposed coordinate partitioning. Section five drafts problems associated to the stability of numerical integrations. Section sixth presents the paper-dedicated modal-based adjustment of the Rayleigh-based model of damping. Section seven presents the numerical model, the tests, and their selected results. Finally, the last section presents conclusions and perspectives.

2   Fundamental Formulas of Kinematics and Dynamics of Multibody Modelling

In the paper, we limit the research to the classic multibody models. We consider, the system is built of non-deformable bodies and massless joints. Allowed relative displacements occur in the joints, and the joints are the single-degree-of-freedom massless elements. The joints' displacements are assumed as the system generalized coordinates. The descriptive assumption is the acceptance of significant magnitudes of the joint displacements. When the idea of bodies and joints is introduced, we can recall the concept of a kinematical chain (Fig. 1a), defined as a sequence of bodies interconnected by joints. Recalling [1, 10, 12], it allows us to introduce the idea of the succession order and the numbering (Fig. 1a). From the recalled bibliographic positions, readers may also refer to the concept of closed kinematical chains.
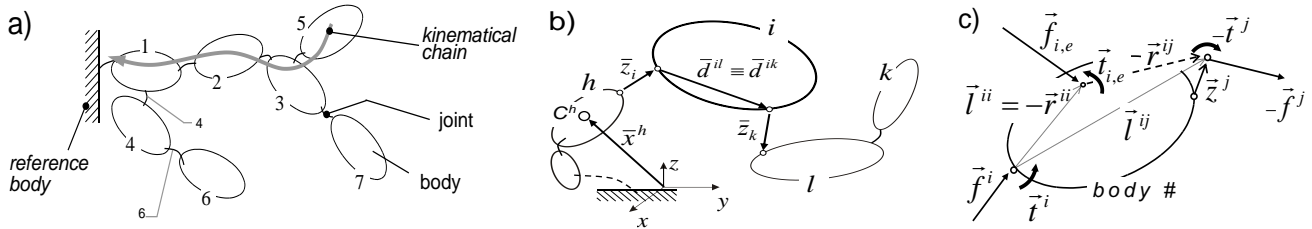
Figure 1: Elements of multibody system structure: joints, bodies and numbering (a); geometrical dimensions of the system and multi-optional description of geometrical distances at the body (b); geometrical parameters of body #i and interactions acting on the body (c)

Let us introduce, $\bar{x}^i$, as the vector of the absolute position of the mass center, C^i, with respect to the origin of the frame fixed to the reference body (see Fig. 1b), as well as the symbol, $\boldsymbol{T}^i$, as the absolute orientation matrix of the body-fixed frame with respect to the frame fixed to the reference body. We may calculate them as sum and product of the body/joint relative parameters. Their time derivatives allow us to write the velocity and acceleration formula. It leads to [1, 3, 10, 12]:

$$\bar{x}^i = \sum_{j:j\leq i} (p^k \cdot \bar{a}^k + \bar{d}^{ji}) = \sum_{j:j\leq i} \bar{l}^{ji} \quad ; \quad \boldsymbol{T}^i = \prod_{j:j\leq i} \boldsymbol{R}^j ; \tag{2ab}$$

$$\dot{\bar{x}}^i = \sum_{k:k\leq i} (\dot{p}^k \cdot \bar{a}^k + \bar{\omega}^k \times \bar{l}^{ki}) \quad ; \quad \bar{\omega}^i = \sum_{k:k\leq i} \dot{\varphi}^k \cdot \bar{e}^k ; \tag{3ab}$$

$$\ddot{\bar{x}}^i = \sum_{k:k\leq i} (\ddot{p}^k \cdot \bar{a}^k + \dot{\bar{\omega}}^k \times \bar{l}^{ki} + 2\dot{p}^k \cdot \bar{\omega}^k \times \bar{a}^k + \bar{\omega}^k \times (\bar{\omega}^k \times \bar{l}^{ki})) \quad ; \quad \dot{\bar{\omega}}^i = \sum_{k:k\leq i} (\ddot{\varphi}^k \cdot \bar{e}^k + \dot{\varphi}^k \cdot \bar{\omega}^k \times \bar{e}^k) , \tag{4ab}$$

where: $\bar{a}^j$ – unit vector of the line of the translational motion at joint #j (it is the zero vector for rotational joints); $\bar{e}^j$ – unit vector collinear to axis of rotations at joint #j (it is the zero vector, if translational joint is considered).

To develop the system dynamics equations, we shall cut all the joints and shall introduce the joints' interactions to replace all the cut connections (Fig. 2b). Then, for each of the obtained free-body diagrams, we shall write Newton/Euler dynamics equations [1, 3, 10, 12]:

$$m^i \cdot \ddot{\bar{x}}^i = \bar{f}^i + \bar{f}^{i,e} - \sum_{j\in i^+} \bar{f}^j \quad ; \quad \bar{\omega}^i \times (\bar{\bar{I}}^i \cdot \bar{\omega}^i) + \bar{\bar{I}}^i \cdot \dot{\bar{\omega}}^i = \bar{t}^{i,e} + \bar{r}^{ii} \times \bar{f}^i + \bar{t}^i - \sum_{j\in i^+} \bar{t}^j - \sum_{j\in i^+} \bar{r}^{ij} \times \bar{f}^j , \tag{5ab}$$

where: m^i – mass of body #i; $\bar{\bar{I}}^i$ – its tensor of moments of inertia (calculated about the centre of mass of this body); $\bar{f}^i, \bar{t}^i$ – joint force and torque at the cut joint #i that act on body #i, $\bar{f}^{i,e}$ – net external force applied at the mass centre of body #i; $\bar{t}^{i,e}$ – net external torque acting on body #i.

To obtain the required/explicit form of the dynamics equations, we shall accompany the obtained dynamics eqs (5) with the velocity eqs (3) and the acceleration eqs (4). Next, we shall eliminate the successors' forces and torques. We shall do it by use of the standard backward evaluation. Finally, we shall project their components on the directions of mobility of the joints (the components of the force, $\bar{f}^i$, on the, $\bar{a}^i$, vector and the components of the torque, $\bar{t}^i$, on the, $\bar{e}^i$, vector, respectively). Finally, we shall factor out the joint accelerations, i.e., we shall collect all the components in front of the accelerations as elements of the mass matrix. Thanks of it, we can write the obtained formulae in the standard form,

$$\boldsymbol{M}^b \cdot \ddot{\boldsymbol{q}}^b + \boldsymbol{F}^b = \boldsymbol{Q}^b . \tag{6}$$

where: $\boldsymbol{q}^b$ – $n_b \times 1$ matrix of generalize coordinates of the system; $\boldsymbol{M}^b = \boldsymbol{M}^b(\boldsymbol{q}^b)$ – $n_b \times n_b$ mass matrix of the system (nonlinear to $\boldsymbol{q}^b$); $\boldsymbol{F}^b = \boldsymbol{F}^b(\dot{\boldsymbol{q}}^b, \boldsymbol{q}^b)$ – $n_b \times 1$ matrix of velocity based inertial terms of the system (nonlinear to $\boldsymbol{q}^b$ and $\dot{\boldsymbol{q}}^b$); $\boldsymbol{Q}^b = \boldsymbol{Q}^b(\dot{\boldsymbol{q}}^b, \boldsymbol{q}^b, \boldsymbol{f}_e, \boldsymbol{t}_e, t)$ – $n_b \times 1$ matrix of the generalized forces of the system; $\boldsymbol{f}_e, \boldsymbol{t}_e$ – external forces and torques, t - time.

Developing the final formula, we shall remain that for mobile systems all the body geometrical distances and the body inertia parameters remain constant uniquely in their local element-fixed systems and should be recalculated to the global one using the time-dependent orientation matrices at each step of the integration.

3 Fundamental Formulas of Finite-Elements Modelling

In the paper, we assumed that the tested deformable detail belongs to the motionless base of the system. To express its deformations, we shall select a finite set of points belonging to this detail. We call them *nodes* and we shall treat their displacements as the system's generalized coordinates. As being points, each node has three degrees of freedom relative to the base (only translational degrees) (Fig. 2a). In several applications, displacements of selected cross sections or displacements of the point-associated planes are investigated instead of displacements the points themselves (Fig 2b). In several particular situations, if selected modes of deformations are assumed as negligible/locked, the investigated number of the degrees could be lower (e.g., for planar bended beam elements, longitudinal displacements are negligible, and two degrees of freedom are sufficient).
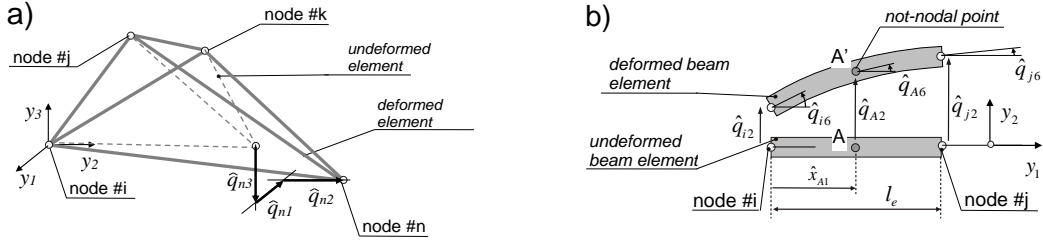
Figure 2: Exemplary finite elements: tetragonal element (a); beam element and displacements of its points (of its nodes and of its generic point *A*) (b)

Let us investigate a generic finite element, *#e*. We number its nodes as *#ei* , $i \in \{1,2,3, ...\}$. For each of the nodes, we shall write two matrices: a matrix of its displacements and a matrix of its loads resolved in the system associated with the element:

$$\widehat{\boldsymbol{q}}^{ei} = col\left(\hat{q}_x^{ei}, \hat{q}_y^{ei}, \hat{q}_z^{ei}\right) \ , \qquad \widehat{\boldsymbol{P}}_{ei} = col\left(\hat{P}_x^{ei}, \hat{P}_y^{ei}, \hat{P}_z^{ei}\right) \ , \qquad (6)$$

where: $\hat{q}_c^{ei}$ – translational displacement of the node *#ei* along *c* axis, $c \in \{x, y, z\}$ (Fig. 3a); $\hat{P}_c^{ei}$ – component of the force at the node *#e1* collinear to axis *c*. Following it, the matrices of the displacements and loads are [1, 3, 5, 13, 14]:

$$\widehat{\boldsymbol{q}}^{e} = col\left(\widehat{\boldsymbol{q}}^{e1}, \widehat{\boldsymbol{q}}^{e2}, ...\right) \ ; \qquad \widehat{\boldsymbol{P}}^{e} = col\left(\widehat{\boldsymbol{P}}^{e1}, \widehat{\boldsymbol{P}}^{e2}, ...\right) \ . \qquad (7)$$

The principal constitutive assumption of the method states that if we investigate a continuous property of the element, we can express it as a linear combination of measures of this property taken at the nodes of the finite element. The constant factors of this linear formula depend on the relative position of the investigated point measured relative to the nodes. Displacement is a typical example of such continuous property, therefore, any displacement of the generic point *A* , denoted here as $\hat{\boldsymbol{\Delta}}^A \equiv \hat{\boldsymbol{\Delta}}$, can be written as [1, 3, 5, 13],

$$\widehat{\boldsymbol{\Delta}} = \widehat{\boldsymbol{N}}^e \cdot \widehat{\boldsymbol{\Delta}}^e = \widehat{\boldsymbol{N}}^e \cdot \widehat{\boldsymbol{q}}^e \ ; \qquad \hat{\boldsymbol{v}} = \dot{\widehat{\boldsymbol{\Delta}}} = \widehat{\boldsymbol{N}}^e \cdot \dot{\widehat{\boldsymbol{q}}}^e, \qquad (8ab)$$

where: $\widehat{\boldsymbol{\Delta}}^e = col\left(\hat{\Delta}_x^{e1}, \hat{\Delta}_y^{e1}, \hat{\Delta}_z^{e1}, \hat{\Delta}_x^{e2}, ...\right)$ – vector of the nodal displacements; $\widehat{\boldsymbol{N}}^e = \left[\widehat{\boldsymbol{N}}^{e1}, \widehat{\boldsymbol{N}}^{e2}, ...\right] = \left[\widehat{N}_x^{e1}, \widehat{N}_y^{e1}, \widehat{N}_z^{e1}, \widehat{N}_x^{e2}, ...\right]$ – matrix of the components of shape functions, associated with the assumed type of the element.

Keeping in mind that the shape functions depend on the relative position of the point (they are not expressed as functions of time or nodal displacements), thus eq. (8b) expresses the formula of velocity of the generic point [1, 3, 5, 13]. What is more, operations on the displacement functions (8a) allows us to calculate the element-associated strains, $\hat{\boldsymbol{\varepsilon}}$. We may calculate these strains using the linear operator of differentiations, $\boldsymbol{\Gamma}_l$. Also, with use of stress-strain formula we may calculate associated stresses, $\hat{\boldsymbol{\sigma}}$. Details of the used stress and strain formulae depend significantly on the assumed stress/strain configuration (details can be found in [1, 3, 5, 13]). The obtained strain and stress formulae allow us to calculate the total energy of the deformation, U^e, accumulated in the investigated finite element and the velocity formula (8b) allow us to calculate the total kinetic energy, E^e. We may write them as [1, 3, 5, 13]

$$E^e = \frac{1}{2}\int_{m^e} \hat{\boldsymbol{v}}^T \cdot \hat{\boldsymbol{v}} \cdot dm \ , \qquad U^e = \frac{1}{2}\int_{V^e} \hat{\boldsymbol{\varepsilon}}^T \cdot \hat{\boldsymbol{\sigma}} \cdot dV \ , \qquad (9ab)$$

Thanks to the cumulative property of the kinetic and potential energy, we may calculate the total energies as sums of the elements' energies. then, we shall factor out the joint velocities in the kinetic energy formula and the joint displacements in the deformation energy formula, i.e., we shall collect all the components in front of the velocities as elements of the mass matrix and in front of the displacements as elements of the elasticity matrix. Finally, we shall eliminate the rows and columns corresponding to the locked nodes (constrained points of the detail), and the final form of equations is [1, 3, 5, 13]:

$$\boldsymbol{M}^c \cdot \ddot{\boldsymbol{q}}^c + \boldsymbol{K}^c \cdot \boldsymbol{q}^c = \boldsymbol{P}^c \ , \qquad (10)$$

or if one intends to complement it a certain amount of damping, it leads to,

$$\boldsymbol{M}^c \cdot \ddot{\boldsymbol{q}}^c + \boldsymbol{C}^c \cdot \dot{\boldsymbol{q}}^c + \boldsymbol{K}^c \cdot \boldsymbol{q}^c = \boldsymbol{P}^c \ , \qquad \widehat{\boldsymbol{\Delta}} = \widehat{\boldsymbol{N}}^{ec} \cdot \widehat{\boldsymbol{q}}^c \ , \qquad (11ab)$$

where: $\boldsymbol{q}^c$ – $n_c \times 1$ matrix of generalize coordinates of the finite-element part; $\boldsymbol{M}^c = const - n_c \times n_c$ mass matrix of the finite-element part; $\boldsymbol{C}^c = const - n_c \times n_c$ damping matrix of the finite-element part; $\boldsymbol{K}^c = const - n_c \times n_c$ elasticity matrix of the finite-element part; $\boldsymbol{P}^c = \boldsymbol{P}^c(\dot{\boldsymbol{q}}^c, \boldsymbol{q}^c, \boldsymbol{f}_e, \boldsymbol{t}_e, t)$ – $n_c \times 1$ matrix of the generalized forces of the finite-element part.

4 Constraint Equations Used to Express the Contacts between the Multibody and the Beam

In the paper, we restrict the tests to a pointwise contact. The contact connects a vertex of a rigid body of the multibody and

a point located at the neutral axis of the beam being a part of the reference body. We may specify two cases of the contact.

4.1 The Pin Contact

In the present case, we model a multibody vertex constantly fixed to a given point of the modelled beam, i.e., the longitudinal position of the contact point is constant along the modelled beam. The only allowable motions are the rotations of the pin and the translations resulting from the beam deformations. If we focus on the relative position of the contact point along the beam (measured respectively to the nodes), the aforesaid relative position is time-invariant. For generality, let us assume that we locate the contact point at a not-nodal point of the deformable detail. We may write the resulting equations as:

$$\Phi_1 \equiv \Phi_1^{fb} = r_{p1} - r_{p1}^b(\boldsymbol{q_b}) = 0 \quad ; \qquad \Phi_2 \equiv \Phi_2^{fbc} = r_{p2}^c(\boldsymbol{q_c}) - r_{p2}^b(\boldsymbol{q_b}) = 0 , \qquad (12ab)$$

where: r_{p1} – longitudinal position of the investigated point at the surface of the elastic body (constant); $r_{p1}^b(\boldsymbol{q_b})$ – longitudinal position of the vertex of the multibody element; $r_{p2}^c(\boldsymbol{q_c})$ – vertical position of the point at the surface of the elastic body; $r_{p2}^b(\boldsymbol{q_b})$ – vertical position of the vertex of the multibody element.

4.2 The Slider-Pin Contact

In the slider-pin case, the investigated vertex of the multibody element can slide along the neutral axis of the investigated beam. The relative position of the contact point is permanently changing respectively to the nodes (in its deformed state, as well as in its non-deformed reference configuration, also). Since there is no constraint in the longitudinal direction, and the common displacement in the vertical directions is the only considered, we may write the resulting constraint equation as:

$$\Phi_3 = \Phi^s = r_{p2}^{cb}(\boldsymbol{q_c}, \boldsymbol{q_b}) - r_{p2}^b(\boldsymbol{q_b}) , \qquad (13)$$

where: r_{p2}^{cb} – vertical position of the contact point at the beam neutral axis; r_{p2}^b – vertical position of the rigid-body vertex.

Let us point out a critical difference between the pin and pin-slider constraints. If we focus on the relative position of the contact point respectively to the nodes (i.e., the longitudinal location of the point at the neutral axis of the beam) it result directly from the longitudinal position of the multibody vertex, thus, it is explicit function of multibody coordinates. Consequently, the vertical position of the contact point at the beam axis depends on both types of the coordinates. Firstly it depends on the coordinates of the finite element (since the vertical displacement is a linear combination of displacements of nodes). But secondly, it also depends on the multibody coordinates (since the shape functions depends on the relative position of the contact point respectively to the nodes, and the relative position is the function of the multibody coordinates).

4.3 Reaction forces and reaction free formula

The two mathematically different systems interact. Selected points of their elements are in contact. To model it, we shall simultaneously solve numerous problems. Firstly, we need a geometry-based algorithm able to find locations of the potential contact point. Secondly, we need a model of the interaction. This model shall articulate the principal physical phenomena of the examined contact. From the point of view of the dynamics, if a single contact appears, one can write the force-interconnected equations as [3, 17, 18]:

$$\boldsymbol{M^b} \cdot \ddot{\boldsymbol{q}}^b + \boldsymbol{F^b} + \boldsymbol{J_b} \cdot N = \boldsymbol{Q^b} \quad ; \qquad \boldsymbol{M^c} \cdot \ddot{\boldsymbol{q}}^c + \boldsymbol{C^c} \cdot \dot{\boldsymbol{q}}^c + \boldsymbol{K^c} \cdot \boldsymbol{q^c} + \boldsymbol{J_c} \cdot N = \boldsymbol{P^c}, \qquad (14ab)$$

where: $N = N(\Delta_n, \dot{\Delta}_n)$ – the investigated normal component of the contact force; $\boldsymbol{J_b} = \partial \Delta_n / \partial \boldsymbol{q_b}$ – Jacobian of the position of the contact point with respect to the coordinates of the multibody system; $\boldsymbol{J_c} = \partial \Delta_n / \partial \boldsymbol{q_c}$ – Jacobian of the position of the contact point with respect to the coordinates of the finite-element part.

A natural alternative to the contact force method is the method focused on constraint equations, extended with idea of the Lagrange's multipliers. If one applies this method, the resulting dynamics can be expressed by the following set of differentially-algebraic equations [1, 3, 15, 16]:

$$\boldsymbol{M^b} \cdot \ddot{\boldsymbol{q}}^b + \boldsymbol{F^b} + \boldsymbol{J_b^\Phi} \cdot \lambda = \boldsymbol{Q^b} , \qquad (15a)$$
$$\boldsymbol{M^c} \cdot \ddot{\boldsymbol{q}}^c + \boldsymbol{C^c} \cdot \dot{\boldsymbol{q}}^c + \boldsymbol{K^c} \cdot \boldsymbol{q^c} + \boldsymbol{J_c^\Phi} \cdot \lambda = \boldsymbol{P^c} , \qquad (15b)$$
$$\Phi = 0 . \qquad (15c)$$

where: $\boldsymbol{\Phi} = \boldsymbol{\Phi}(\boldsymbol{q^b}, \boldsymbol{q^c})$ – the examined constraint function that express the magnitude of the relative penetration (function of the multibody and finite-elements coordinates); λ - unknown Lagrange multiplier; $\boldsymbol{J_b^\Phi} = \partial \boldsymbol{\Phi} / \partial \boldsymbol{q^b}$ - Jacobian of the constraint function with respect to the coordinates of the multibody system; $\boldsymbol{J_c^\Phi} = \partial \boldsymbol{\Phi} / \partial \boldsymbol{q^c}$ – Jacobian of the relative penetration with respect to the coordinates of the finite-element part.

The constitutive principle of calculating the multipliers implemented inside eq. (15) refers directly to the request of zeroing the relative accelerations of the contacting points (i.e. to zeroing the second time derivative of the constraint equation (15c)). The obtained values of the multipliers correspond to the contact force able to drive both systems with such accelerations of joints, which lead to acceleration of points that are equal at the contact point. As pointed out in [16], the multipliers method defeats most of the troubles of the ill-conditioning. Also, with the multipliers method, the geometrical conditions of the physical contact are fulfilled precisely [16], as well as stability of the system is achieved by fulfilling the energy preservation and energy decay [15].

In the next step, we shall focus on coordinate partitioning and the elimination of Lagrange's multipliers. The initial partitioning step consists of the coordinate partitioning. It splits the system coordinates into dependent and independent ones. It also results in an associated subdivision of the Jacobian matrix. Since we shall limit the dependent coordinates to the multibody part, we can recall the initial steps of the classic multibody coordinate partitioning [19]. We can reorder the numbering of the dynamics equations (15a) and reorder the numbering of the multibody coordinates. After the reorder, we

may rewrite the dynamics equations of the multibody part as:

$$\boldsymbol{M}_{uu} \cdot \ddot{\boldsymbol{u}} + \boldsymbol{M}_{uv} \cdot \ddot{\boldsymbol{v}} + \boldsymbol{F}_u + (\boldsymbol{J}_u^{\Sigma})^T \cdot \boldsymbol{\lambda} = \boldsymbol{Q}_u \quad , \tag{16a}$$

$$\boldsymbol{M}_{vu} \cdot \ddot{\boldsymbol{u}} + \boldsymbol{M}_{vv} \cdot \ddot{\boldsymbol{v}} + \boldsymbol{F}_v + (\boldsymbol{J}_v^{\Sigma})^T \cdot \boldsymbol{\lambda} = \boldsymbol{Q}_v \quad . \tag{16b}$$

Then we may calculate Lagrange's multipliers from (16b) and we shall introduce this formula to (16a) to eliminate the multipliers. Next we shall eliminate accelerations of the dependent coordinates. Recalling the differentiated constraint equations (15c) and applying the introduced coordinate partitioning to the obtained linear equations at the acceleration level, the examined accelerations of the dependent coordinates can be resolved as explicit functions of the independent ones. It allow us to eliminate the obtained accelerations, $\ddot{\boldsymbol{v}}$, from (16a). To complete the dynamics equations of our system, we have to expand the set with the equations of dynamics of the elastic part. To obtain it, we shall apply the explicit formula of Lagrange's multiplayers calculated from (16b) to eliminate the multipliers from (15b). Summarising the obtained formulae, we can write the dynamics in independent coordinates as:

$$\begin{cases} \boldsymbol{M}_{11} \cdot \ddot{\boldsymbol{u}} + \boldsymbol{M}_{12} \cdot \ddot{\boldsymbol{q}}_c + \boldsymbol{F}_1 = \boldsymbol{Q}_1 \; ; \\ \boldsymbol{M}_{22} \cdot \ddot{\boldsymbol{q}}_c + \boldsymbol{C}_c \cdot \dot{\boldsymbol{q}}_c + \boldsymbol{K}_c \cdot \boldsymbol{q}_c + \boldsymbol{M}_{21} \cdot \ddot{\boldsymbol{u}} = \boldsymbol{P}_2 \; , \\ \boldsymbol{\Phi}(\boldsymbol{u}, \boldsymbol{v}, \boldsymbol{q}_c) = \boldsymbol{0} \end{cases} \tag{17}$$

More details about the elimination procedure and about the final matrices, readers can find in [3].

5 Stability of Numerical Integration

There is a number of numerical methods that are trying to estimate evolution of integrated functions. They shall do it on the basis of values of the function (and derivatives) known in previous steps of the algorithms. The most popular/classical are:

- forward evaluation (Euler method): $y_n - y_{n-1} - h \cdot \dot{y}_{n-1} = 0$;
- backward evaluation: $y_n - y_{n-1} - h \cdot \dot{y}_n = 0$;
- explicit midpoint: $y_n - y_{n-2} - 2h \cdot \dot{y}_{n-1} = 0$;
- trapezoid rule: $y_n - y_{n-1} - \frac{h}{2} \cdot (\dot{y}_n + \dot{y}_{n-1}) = 0$;
- linear multistep method: $\sum_0^k \alpha_i \cdot y_{n-i} + \sum_0^m \beta_i \cdot \dot{y}_{n-i} = 0$,

where, h is the integration step (time interval). As it is commonly reported, the choices of the parameter h significantly affects the convergence and stability of the integration algorithms. Examples of unstable/non-converging results of numerical integration are presented in fig 3.
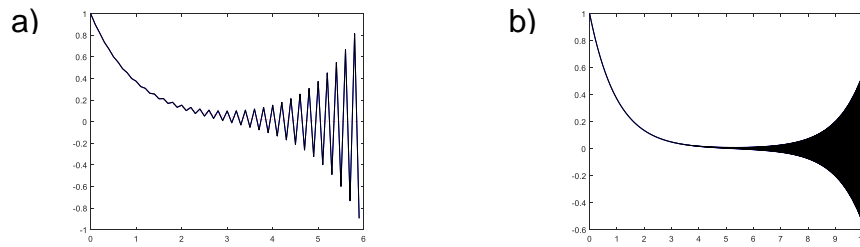
Figure 3: Unstable numerical integration (explicit midpoint algorithm; $\dot{y} = -y$; $y_0 = 1$): h=0.1 (a); h=0.01 (b)

In most of the cases, right estimation of the parameter is a straightforward problem. Exemplary, if linear differential equations are considered (the case tested in the next part of the paper), we shall write its associated differential equation as:

$$\dot{y} = \lambda \cdot y \; ; \qquad y(0) = 1. \tag{18}$$

Examined equation may be solved analytically, its exact solution and its first derivative are $y(t) = e^{\lambda \cdot t}$; $\dot{y}(t) = \lambda \cdot e^{\lambda \cdot t}$. Accordingly, if we test algorithm of the forward evaluation and this analytical solution is substituted there, one obtains:

$$e^{\lambda \cdot (t+h)} = e^{\lambda \cdot t} + h \cdot \lambda \cdot e^{\lambda \cdot t} \; ; \tag{19a}$$

$$e^{\lambda \cdot h} = 1 + h \cdot \lambda = 0 \; ; \tag{19b}$$

$$y_n = e^{\lambda \cdot n \cdot h} = (1 + h \cdot \lambda)^n. \tag{19c}$$

If the coefficient, λ, is negative, the obtained analytical solution attempts to zero. To obtain identical behaviour of the numerical one, we shall expect that, $|1 + h \cdot \lambda| < 1$, i.e., $h < -2/\lambda$. Similar formulae can be obtained for the other algorithms pointed-out above. Accordingly, we may introduce a parameter that indicates rapidity of decay of solutions as t increases. We call it *stiffness of the differential equation*. Some numerical methods, which are generally effective for non-stiff systems, fail for the stiff ones, or stability of their solution can only be achieved for very small h.

6 Adjustment of the Rayleigh-based damping

Let us look on the dynamics equation expressed in their nodal formulation (10), and assume that the generalized forces are absent. Its analytical solution $\boldsymbol{q}^c(t) = \boldsymbol{\Psi} \cdot \sin(\omega \cdot t)$, i.e., we need a column matrix, $\boldsymbol{\Psi}$, that fulfils the following equation,

$$(-\omega^2 \cdot \mathbf{M}^c + \mathbf{K}^c) \cdot \boldsymbol{\Psi} = \boldsymbol{0} \; , \tag{20}$$

its non-trivial solution exist uniquely, if

$$det(-\omega^2 \cdot \mathbf{M}^c + \mathbf{K}^c) = 0 \; . \tag{21}$$

Since (21) is a polynomial of order n respectively to ω^2, its solution contains *n* various values of ω_j^2, and thus, we shall obtain *n* various shape-modes, $\boldsymbol{\Psi}_j$. All these modes are mass and stiffness orthogonal [8, 14, 20]. Moreover, assuming the shape modes as mass-normalized, we shall conclude that:

$$\boldsymbol{\Phi}^T \cdot \boldsymbol{M}^c \cdot \boldsymbol{\Phi} = \boldsymbol{I} \; ; \qquad\qquad \boldsymbol{\Phi}^T \cdot \boldsymbol{K}^c \cdot \boldsymbol{\Phi} = diag\left(\omega_j^2\right). \tag{22}$$

Let we use the classic transformation formula, $\boldsymbol{q}^c = \boldsymbol{\Phi} \cdot \boldsymbol{q}^m$ (coordinates $\boldsymbol{q}^m$ are called modal coordinates). Thanks to the property (22), the dynamics equations (10) can be written in their decupled scalar form [9, 14, 20],

$$\ddot{q}_j^m + \omega_j^2 \cdot q_j^m = P_j^m \; . \tag{23}$$

What is more, if the Rayleigh damping matrix is used, the resulting modal-damping matrix is also a diagonal one. Accordingly, if one examinee a given frequency, ω_j, its decupled dynamics equation is [9, 8, 14, 20]:

$$\ddot{q}_j^m + \left(\alpha + \beta \cdot \omega_j^2\right) \cdot \dot{q}_j^m + \omega_j^2 \cdot q_j^m = P_j^m \; ; \qquad \text{or} \qquad \ddot{q}_j^m + \zeta_j \cdot c_{jc}^m \cdot \dot{q}_j^m + \omega_j^2 \cdot q_j^m = P_j^m \; ,: \tag{24ab}$$

$$c_{jc}^m = 2\sqrt{k_j \cdot m_j} = 2\sqrt{\omega_j^2} = 2\omega_j \; ; \qquad\qquad \zeta_j = \frac{\alpha}{2} \cdot \omega_j^{-1} + \frac{\beta}{2} \cdot \omega_j \; , \tag{24cd}$$

where: c_{jc}^m - critical damping of the mode; ζ_j –ratio of its modal damping.

Following, if the Rayleigh formula is used, all modes are damped and oscillational motions are present only, if ratios of their critical damping are lower than 1. Comparing it with the typical Rayleigh parameters (e.g., β=3.23·10^{-3} [8]), the oscillated ones are present, if undamped natural angular frequencies are lower than ω_c=619.2. If one investigates beam vibrations, only few of the modes are oscillational. Their majority consist of the overdamped/non-oscillated ones, and we have to operate with the really-high real eigenvalues. A lot of them can be higher than 10^8. Their associated evolutions are express with the function, $\boldsymbol{q}_j = exp\left(-r_j \cdot t\right) \cdot A_j \cdot \boldsymbol{\Phi}_j$, and according to the presence of the multiplicand, $exp\left(-r_j \cdot t\right)$, the mode disappears rapidly, even below the limit of the time of the numerical observation. After the period of its reduction, it stabilizes at its zero value (assuming a time interval of $\Delta t = \cdot 10^{-7}$ s, and a mode with its eigenvalue $r_j = -1.315 \cdot 10^8$, it reduces its amplitude by the factor, $R = exp(-13.15) = 1.95 \cdot 10^6$, i.e., about two million times). According to formula (19), its time step is $h < -2/\lambda = 1.521 \cdot 10^{-8}$. Such tiny integration steps can extremely slow down the integration processes.

Therefore, we have a significant modelling dilemma: if we intend investigates a practical example of a beam, we shall expect that the external load may excite a given high-real-eigenvalue mode. But excited amplitude will be low (since potential energy of its deformation is limited), and its speed will disappear rapidly, and therefore it is not rational to integrate all details of its rapid disappearance. We shall treat it as a process below our observation range. As said in the introduction, we can exclude this numerical problem by using the classical *modal coordinate reduction technique*. We can detect the problematic modes and eliminate them from the numerical model (i.e., assuming their amplitudes as equal zero after the period). The initial and the resulting models will be numerically equivalent. If focusing on the present paper, its main idea is the *modal adjustment of damping coefficients*. According to this idea, we keep all the modes in the model, but we modify their damping ratios. We fit them to the user-proposed time step of integration. We address modifications to the highest ω_j and only to the real eigenvalues. We operate with a user-assumed limit value, ω^l, and with these modes that satisfy the supplementary relation, $\omega_j > \omega^l$. For each of these modes, we maintain the ratios of their modal damping slightly above 1, and with use of (24c), we calculate its diagonal element of the modal damping matrix from the formula:

$$c_{jj}^a = \zeta_j \cdot c_{jc}^m = (1 + l/2) \cdot \left(2 \cdot \omega_j\right) = (2 + l) \cdot \sqrt{k_{jj}^m} \; . \tag{25}$$

Its associated eigenvalue, r_j, can be calculated from the root of the quadratic equation (24b). Since the modal damping is close to critical one, then the root-square term of (26) is insignificant, and the following simplification is valid,

$$r_j = -\frac{1}{2}\zeta_j \cdot c_{jc}^m \pm \frac{1}{2}\sqrt{\left(\zeta_j \cdot c_{jc}^m\right)^2 - 4 \cdot \omega_j^2} \approx -\frac{1}{2}\zeta_j \cdot c_{jc}^m \approx -\frac{\beta}{2} \cdot \omega_j^2 \; . \tag{26}$$

Accordingly, if obtained eigenvalue is lower than the user-assumed limit value, r^l, there exist a time step, h^l, for which the initial and the modified models are numerically equivalent. Appointed adjustment is straightforward when one performs it at the level of the modal coordinates. To convert it to the domain of the nodal coordinates, we invoke the inverted formula to (78), and we write it as,

$$\boldsymbol{C}^c = \left(\boldsymbol{M}^c \cdot \boldsymbol{\Phi}\right) \cdot \boldsymbol{C}^m \cdot \left(\boldsymbol{\Phi}^T \cdot \boldsymbol{M}^c\right) \; . \tag{27}$$

More details about the adjustment one can find in [21]

7   Numerical example

Figure 4a shows the sketch of the examined structure and its main geometrical parameters. It consist of a single multibody system and two elastic beams. The beams are 1 m long. We attached them to the base with use of two pin supports, a pin at each end of the beam. 50 beam elements discretize any of the beams (relatively low meshing). We use the absolute nodal formulation to model the beams. Their cross-sections are squares. The sides of the squares are: a = 4.5; 5 and 5.5 mm long (depending on the performed test). The density is, $\rho = 7.86 \cdot 10^3$ kg/m^3; Young modulus, $E = 2.1 \cdot 10^{11}$ Pa/m^2. We build their numerical models according to the rules presented in section 3.

Figure 4b presents the multibody segment. We use seven bodies to build it. The two initial bodies are fictitious (massless and dimensionless). They composes the three initial degrees of freedom. Body #3 refers to the moving platform. Its mass and moment of inertia are m_3=10 kg and I_3=0.5 kg·m^2, respectively. Slider-pin constraints connect the body with the elastic

beam #2 at point *CP*#2 (contr. #2 in Fig 5b). Body #4 represents the first arm. It connects the platform with the elastic beam #1 using a pin constraint (contr. #1 in Fig 5b). Body #4 is a rigid beam. Its mass and moment of inertia are m_4= 3.5 kg and I_4= 0.04 kg·m^2, respectively. We constructed the model of its dynamics according to the rules presented in section 2.
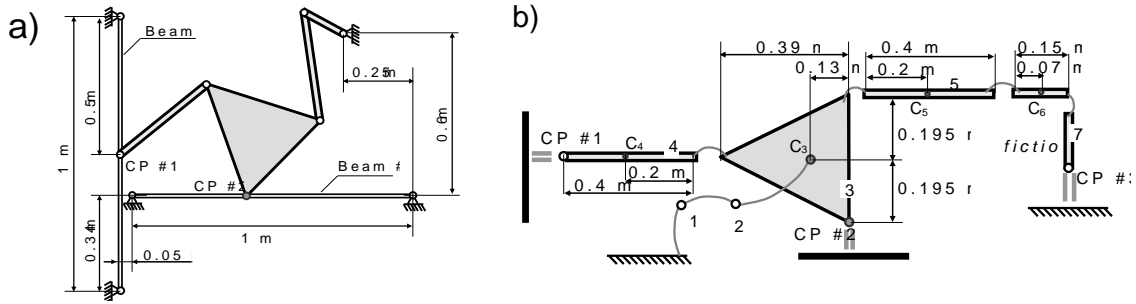

Figure 4: Details of the investigated structure: sketch of the structure (a); its main geometrical parameters (b)
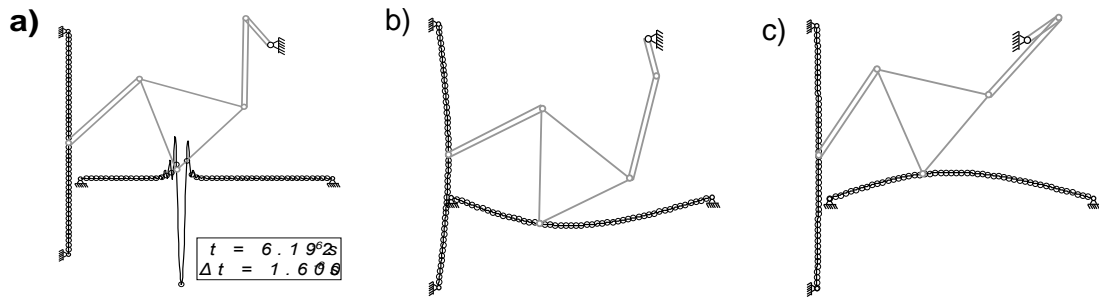

Figure 5: Results of numerical integrations: unstable behavior, original Rayleigh model, $\alpha=\cdot3\cdot10^{-3}$ and β=2.5·10^{-4}, Δt= 1.6·10^{-8} (a); stable behavior of modified system, time step Δt= 1.4·10^{-5}, integrated time t=0.799 s (b); stable behavior of modified system, time step Δt= 1.4·10^{-5}, integrated time t=1 s (c)

The initially-presumed Rayleigh's parameters equal $\alpha=\cdot3\cdot10^{-3}$ and β=1.5·10^{-4}, respectively. With use of them, we make the modal analysis of the beams. We converted their dynamics (2) to the associated state representation (i.e. we introduced associated state vector, $\boldsymbol{y}=col(\boldsymbol{q},\dot{\boldsymbol{q}})$). It leads to [14, 20]:

$$\boldsymbol{I}\cdot\dot{\boldsymbol{y}}-\boldsymbol{B}\cdot\boldsymbol{y}=\boldsymbol{0}\quad;\qquad \boldsymbol{B}=\begin{bmatrix} \boldsymbol{0} & \boldsymbol{I} \\ -\boldsymbol{M_c^{-1}}\cdot\boldsymbol{K_c} & -\boldsymbol{M_c^{-1}}\cdot\boldsymbol{C_c} \end{bmatrix}.. \qquad (28)$$

Factors of their solution, r_j, and the modal shapes, $\boldsymbol{\Phi}_j$, are obtained from the associated eigenvalue problem. We collected their selected values of the calculated eigenvalues, frequencies, and damping ratios in Table 1. Obtained results certified that the number of oscillations is low (there are only 12 oscillations). The dominant part are the real modes. When focusing on the last rows, the moduli of their eigenvalues are high than 10^8.

Table 1. Eigenvalues, frequencies, and damping ratios for the non-adjusted and adjusted systems

#	eigenvalues		ω_{jo} [1/s]	ζ_j [%]	ω_j [1/s]	#	eigenvalues		ω_{jo} [1/s]	ζ_j [%]	ω_j [1/s]
	real	imaginary					real	imaginary			
1	$-4.085\cdot10^{-1}$	$-7.367\cdot10^1$	11.72	0.55	11.72	1	-3.680	$-7.357\cdot10^1$	11.71	5.00	11.72
3	-6.533	$-2.950\cdot10^2$	46.96	2.21	46.97	3	$-1.474\cdot10^1$	$-2.947\cdot10^2$	46.91	5.00	46.97
5	$-3.323\cdot10^1$	$-6.648\cdot10^2$	105.80	4.99	105.94	5	$-3.325\cdot10^1$	$-6.648\cdot10^2$	105.80	5.00	105.93
7	$-1.0574\cdot10^2$	$-1.183\cdot10^3$	188.22	8.91	188.98	7	$-1.057\cdot10^2$	$-1.183\cdot10^3$	188.22	8.91	188.98
9	$-2.604\cdot10^2$	$-1.845\cdot10^3$	293.66	13.98	296.57	9	$-2.604\cdot10^2$	$-1.845\cdot10^3$	293.66	13.98	296.57
...	...	...	...	...	...	...	...	...	...	...	...
60	$-6.672\cdot10^3$	0	-	-	-	60	$-6.672\cdot10^3$	0	-	-	-
61	$-6.672\cdot10^3$	0	-	-	-	61	$-6.672\cdot10^3$	0	-	-	-
...	...	...	...	...	...	...	...	...	...	...	...
196	$-1.237\cdot10^8$	0	-	-	-	196	$-1.370\cdot10^5$	0	-	-	-
197	$-1.270\cdot10^8$	0	-	-	-	197	$-1.370\cdot10^5$	0	-	-	-
198	$-1.295\cdot10^8$	0	-	-	-	198	$-1.370\cdot10^5$	0	-	-	-
199	$-1.310\cdot10^8$	0	-	-	-	199	$-1.370\cdot10^5$	0	-	-	-
200	$-1.315\cdot10^8$	0	-	-	-	200	$-1.370\cdot10^5$	0	-	-	-

Header spanning row: $\alpha=\cdot3\cdot10^{-3}$ and β=1.5·10^{-4} - non-adjusted | $\alpha=\cdot3\cdot10^{-3}$ and β=1.5·10^{-4} - adjusted

To verify the potential risk of the loss of stability, we use the classic algorithm of the forward evaluation, and we integrate the process with the time step of, Δt= 1.6·10^{-8}. Figure 5a presents the obtained result. After a number of steps we observed loss of the stability. In the next test, we verified effectiveness of the proposed adjustment. We started with the previously-used Rayleigh formula and parameters, we adjust the damping according to (25), and we convert the resulting matrix to its nodal representation. The used parameters are: $\omega^l = 10^5$; l = 0.1. We reuse (28) to perform the modal analysis. Table 1

presents the obtained eigenvalues, frequencies, and damping ratios. As we can see, the highest of the obtained eigenvalues is, r_{200}=-1.370·10^5, and the number of decaying oscillations is preserved (as well as their frequencies and damping ratios). In the subsequent test, we perform the time simulations of the modified systems. We use the previously-proposed algorithm of the forward evaluation. We detected the unstable behaviour with the time step of, Δt= 1.5·10^{-5}, while with the time step, Δt= 1.4·10^{-5}, the system's behaviour does not indicate any instability (see Fig. 5bc). According to it, we may conclude that the introduced adjustment allows us to increase the time step about 1000 times compared to the initial simulations).

8   Conclusions

Design of collective multibody/finite-elements models is a technically and academically inquiring problem. The heterogeneity of the used coordinates and the obtained dynamics equations imply numerous consequences critical in verbalizing the constraint equations. Except for its mathematical diversity, there is a diversity based on the wide range of the time constants expressing the modelled phenomena. The presence of this range becomes significantly decisive in numerical analyses. We have to test phenomena with their time constants of range 10^{-10} (or lower) and we need to observe processes in periods of a few seconds or even minutes. The number of necessary integration steps, and the number of stored results, become numerically impracticable.

The paper's proposed technique of modal modification of the structural damping reduces some numerical defects of the pointed-out numerical problem. We recommend this method as an attractive option to the other standardly-used reductions of the modals. Numerical tests have certified that our algorithm can suggestively reduce time necessary to model the technically interesting processes. Also, it certify its usefulness in the multibody/finite-elements simulations.

9   References

[1] Lipinski K.: Multibody systems with unilateral constraints in application to modelling of complex mechanical systems. Seria Monografie, Vol.123, Gdansk University of Technology Publishing House, Gdansk, Poland (in Polish), 2012.

[2] Bautista A., Montesinos J., Pintado P.: Dynamic interaction between pantograph and rigid overhead lines using a coupled FEM — multibody procedure. Mechanism and Machine Theory, Vol. 97, 100-111, 2016.

[3] Lipinski K., Closed form constraint equations used to express frictionless slip of multibody systems attached to finite elements - application to a contact between a double pendulum and a beam. Applied Sciences-Basel, Vol. 13, 3681, 2023.

[4] Antunes P., Magalhaes H., Ambrosio J., Pombo J., Costa J.: A co-simulation approach to the wheel–rail contact with flexible railway track. Multibody System Dynamics. Vol. 45, 245–272, 2019.

[5] Seo J.H., Kim S.W., Jung I.H., Park T.W., Mok J.Y., Kim Y.G., Cha J.B.: Dynamic analysis of a pantograph-catenary system using absolute nodal coordinates. Vehicle System Dynamics, Vol. 44(8), 615-630, 2006.

[6] Rayleigh L.: Theory of Sound. 1954th ed., Dover Publications, New York, 1877

[7] Shabana A.A.: Vibration of discrete and continuous systems. Springer Nature Switzerland AG, 2019.

[8] Bianchi J.P., Balmes E., Bobillot A., Vermot des Roches G.: Using modal damping for full model transient analysis. Application to pantograph/catenaty vibration. In: Proc. of the Int. Conf. on Adv. Acoustics and Vibration Eng., ISMA 2010, Louvain, Belgium, (2010) 1167-1180

[9] Hall J. F.: Problems Encountered from the use (or misuse) of Rayleigh damping. Earthquake Engineering and Structural Dynamics, Vol. 35(5), 525-545, 2005.

[10] Fisette P., Lipinski K., Samin J.C.: Modelling for the simulation control and optimization of multibody system. In: Advances in Multibody System and Mechatronics, Gratz (Austria), 139-174, 1999.

[11] Tian Q., Flores P., Lankarani H.M.: A comprehensive survey of the analytical, num. and experimental methodologies for dynamics of multib. mech. systems with clearance or imperfect joints. Mech. & Mach. Theory, Vol. 122, 1-57, 2018.

[12] Fisette P., Samin J.C.: Symbolic Modeling of multibody system. Kluwer Acad. Publ., Netherlands, 2003

[13] Zienkiewicz O.C., Taylor R.L.: The finite element method, Vol. 1, 5th ed., Butterworth-Heinemann, Oxford, 2000.

[14] Gawroński W., Kruszewski J., Ostachowicz W., Tarnowski J., Wittbrodt E.: The finite element method in the dynamics of constructions. Arkady, Warszawa, Poland ,(in Polish), 1984.

[15] Bauchau O.A., Bottasso C.L.: Contact conditions for cylindrical, prismatic, and screw joints in flexible Multibody Systems. Multibody System Dynamics, Vol. 5, 251–278, 2001.

[16] Cavalieri F.J., Cardona A., Fachinotti V.D., Risso J.: A finite element formulation for nonlinear 3D contact problem. In: Mecanica Computational Vol XXVI, S. Elaskar, E Pilotta, G. Torres (Eds), 26, Cordoba, Argentina, 1357-1372, 2007.

[17] Ambrosio J.,Pombo J.,Pereira M., Antunes P., Mosca A.: A Computational procedure for the dynamic analysis of the catenary-pantograph interaction in High-speed trains. Journal of Theoretical and Applied Mechanics, Vol.50, 681-699, 2012.

[18] Antuanes P., Ambrosio J., Pombo J., Facchinetti A.: A new methodology to study the pantograph-catenary dynamics in curved railway tracks. Vehicle System Dynamic, Vol. 58(3), 425-452, 2020.

[19] Haug E.J., Yen J.: Generalized coordinate partitioning methods for numerical integration of differential-algebraic equations of dynamics. In: Haug, E.J., Deyo, R.C. (eds) Real-Time Integration Methods for Mechanical System Simulation. NATO ASI Series, vol 69. Springer, Berlin, Heidelberg, 97–114, 1990.

[20] Kruszewski J., Wittbrodt E., Walczyk Z.: Vibrations of mechanical systems in the computer approach. vol. 2, WNT, Warszawa, Poland, (in Polish), 1993.

[21] Lipiński K.: Modal adjustment of Rayleigh based structural damping and coordinate-partitioning algorithm dedicated to frictionless contact constraints between multibody system and structure modelled with finite elements. SSRN Electronic Journal, 2023.